AGU PUBLICATIONS

JGR

Journal of Geophysical Research: Atmospheres

RESEARCH ARTICLE
10.1002/2016JD026256

Key Points:
- The accuracy of the SOM patterns is dependent on the type of extreme event being analyzed, which requires careful consideration
- The SOM training procedure can be modified to produce more accurate patterns and to include a greater diversity of patterns
- The SOM patterns represent the circulation during heat wave events well and can provide additional insight

Supporting Information:
- Supporting Information S1

Correspondence to:
P. Gibson,
peter.gibson@unsw.edu.au

Citation:
Gibson, P. B., S. E. Perkins-Kirkpatrick, P. Uotila, A. S. Pepler, and L. V. Alexander (2017), On the use of self-organizing maps for studying climate extremes, *J. Geophys. Res. Atmos.*, *122*, 3891–3903, doi:10.1002/2016JD026256.

Received 16 NOV 2016
Accepted 27 MAR 2017
Accepted article online 29 MAR 2017
Published online 14 APR 2017

On the use of self-organizing maps for studying climate extremes

Peter B. Gibson[1,2], Sarah E. Perkins-Kirkpatrick[1,2], Petteri Uotila[3], Acacia S. Pepler[1,2], and Lisa V. Alexander[1,2]

[1]Climate Change Research Centre, University of New South Wales, Sydney, New South Wales, Australia, [2]ARC Centre of Excellence for Climate System Science, University of New South Wales, Sydney, New South Wales, Australia, [3]Finnish Meteorological Institute, Helsinki, Finland

Abstract Understanding how climate extremes are sensitive to a changing climate requires characterization of the physical mechanisms behind such events. For this purpose, the application of self-organizing maps (SOMs) has become popular in the climate science literature. One potential drawback, though not unique to SOMs, is that the background synoptic conditions represented by SOMs may be too generalized to adequately describe the atypical conditions that can co-occur during the extreme event being considered. In this paper, using the Australian region as a case study, we illustrate how the commonly used SOM training procedure can be readily modified to produce both more accurate patterns and patterns that would otherwise occur too rarely to be represented in the SOM. Even with these improvements, we illustrate that without careful treatment, the synoptic conditions that co-occur during some types of extreme events (i.e., heavy rainfall and midlatitudinal cyclone occurrence days) risk being poorly represented by the SOM patterns. In contrast, we find that during Australian heat wave events the circulation is indeed well represented by the SOM patterns and that this application can provide additional insight to composite analysis. While these results should not necessarily discourage researchers seeking to apply SOMs to study climate extremes, they highlight the importance of first critically evaluating the features represented by the SOM. This study has provided a methodological framework for such an evaluation which is directly applicable to other weather typing procedures, regions, and types of extreme events.

1. Introduction

While still relatively new to the field of synoptic climatology, the use of self-organizing maps (SOMs) and the diversity of applications continue to increase [*Sheridan and Lee*, 2011]. SOMs are often implemented as a tool for "objective" synoptic weather typing, whereby circulation features in the atmosphere, typically mean sea level pressure (MSLP) or geopotential height patterns, are generalized to a selected number of states. It is intended that the resulting circulation patterns are physically realistic and span a range of circulation features found in the atmosphere but that the resulting number of patterns is sufficiently small to be readily managed in subsequent analysis [*Hewitson and Crane*, 2002]. The circulation patterns obtained from SOMs are often then used to understand linkages between large-scale regional circulation and local meteorological variables (e.g., rainfall or temperature variability) or environmental considerations (e.g., glacier recession or fish migration). As an example, *Gibson et al.* [2016a] examined linkages between SOM-derived circulation patterns and spatial distributions of temperature and potential evapotranspiration in New Zealand and suggested that model-projected circulation changes may manifest as significant nonuniform climatic change in that region.

Increasingly, SOMs are used to study the large-scale atmospheric circulation features that co-occur during extreme events, namely, temperature and rainfall extremes. *Horton et al.* [2015] provided evidence that changes in the frequency of geopotential height patterns since the 1980s have already added to changes in extreme temperature trends in some Northen Hemisphere midlatitudinal regions. *Cassano et al.* [2015] and *Cassano et al.* [2016] examined surface circulation patterns conducive to Arctic winter temperature extremes, while *Loikith and Broccoli* [2015] compared circulation links to North American temperature extremes between observations and climate models. Focusing on rainfall, *Alexander et al.* [2010] found that changes in circulation patterns across parts of southern Australia for the 20th century have likely contributed to decreasing trends in rainfall and rainfall extremes and decreases in "storminess." Similarly, but focusing on South African rainfall, *Lennard and Hegerl* [2015] suggest that some seasonal rainfall trends and seasonal timing of rainfall extremes can be linked to trends in regional circulation patterns. Using a different approach to

studying precipitation extremes, *Swales et al.* [2016] trained SOMs on vertically integrated water vapor transport to examine different delivery mechanisms for extreme rainfall in the U.S.

As with other neural network algorithms, a number of SOM training parameters are required to be specified by the user prior to the training. When trained in sequential mode the SOM training procedure is governed by the learning rate parameter, the neighborhood radius, and the number of iterations performed. For each iteration, the SOM training algorithm compares the input vector (in this case the daily MSLP field) to the best matching node, based on Euclidean distance, to determine a "winning node." This winning node is activated along with surrounding nodes which are organized in a 2-D array, and activated node patterns are iteratively updated to better resemble the input vector. The magnitude by which node patterns are updated is determined by the learning rate parameter, while the number of surrounding nodes activated is determined by the neighborhood radius parameter. Both of these training parameters decrease from a user-defined initial point to a user-defined end point across the training iterations (typically several thousands) such that the SOM converges to a stable solution.

A number of studies have reported that the starting point for the learning rate and neighborhood radius training parameters generally have little influence on the patterns produced in the maps and their associated realism [e.g., *Cassano et al.*, 2006; *Johnson et al.*, 2008; *Alexander et al.*, 2010; *Cassano et al.*, 2015]. By SOM (or node) pattern realism we refer to the degree of similarity between the SOM pattern and the actual daily field (e.g., as measured by a pattern correlation). A common approach in synoptic climatology applications is to allow the radius parameter to decrease monotonically (typically linearly) to 1 and then stop the training at this point. Doing so ensures that throughout the training processes, both the winning and surrounding nodes are updated; this acts to preserve the topological ordering of nodes (i.e., similar nodes are positioned together in the 2-D SOM plane) which is a unique feature of SOMs.

With only a few exceptions [e.g., *Jiang et al.*, 2015], what appears less documented in the synoptic climatology literature is the influence of the end point of the radius parameter. At the point where the radius parameter exactly equals 1, the SOMs approach is shown to be equivalent to K-means clustering as only the "winning node" is updated at each iteration (in contrast the winning node and surrounding nodes) [*Bação et al.*, 2005]. Therefore, an option in the SOM training is to start the SOM training in usual fashion (i.e., with both the winning node and surrounding nodes updated) but in later iterations of the training process allow only the winning node to be updated. This approach was recently applied by *Jiang et al.* [2015] to circulation patterns in eastern Australia, where the authors found advantages over the more traditional SOM training procedure in terms of the average classification error.

Another consequence that arises from allowing the radius parameter to reach 1 (and subsequently to be fixed at 1) during training is that the topological ordering of patterns in the 2-D SOM plane is reduced. The relative importance of SOM pattern realism versus topological ordering will depend on the specific application. For exploratory type analysis where the intention is often primarily to uncover or visualize the underlying structure of the data and to identify relationships between extracted features, the topological features of the SOM are certainly of value. Examples of this type of application include examining coastal ocean currents [*Liu et al.*, 2006], different "flavors" of El Niño–Southern Oscillation [*Johnson*, 2013], and comparing circulation patterns in climate models [e.g., *Gibson et al.*, 2016b], among many others. For later reference we shall refer to this approach as SOMs for projections.

Other applications of SOMs, however, rely more heavily on the extraction of realistic SOM features, with these features subsequently used as clusters to examine links with other meteorological variables [e.g., *Lennard and Hegerl*, 2015; *Huva et al.*, 2015; *Horton et al.*, 2015]. Therefore, attempts to optimize the realism of SOM patterns through training parameters are most relevant. For later reference we shall refer to this approach as SOMs for clustering. Indeed, when using SOMs for studying extremes, if the highly generalized SOM patterns are not able to realistically characterize the synoptic conditions associated with the extreme event, then the relevance of the SOM patterns could be questionable. *Huva et al.* [2015] demonstrate that, without careful treatment, the generalized SOM nodes often do not adequately represent the relevant synoptic circulation features associated with rainfall at major Australian cities and this may lead to erroneous conclusions regarding how circulation patterns have contributed to rainfall trends at these locations. *Lennard and Hegerl* [2015] linked rainfall trends to SOM patterns but also cautioned that the SOM patterns used in their study do not capture closed low-pressure systems known to be linked to heavy rainfall in that region. Similarly, but for

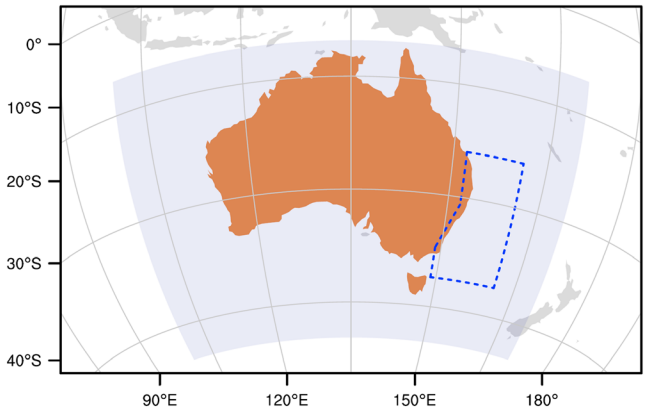

Figure 1. Map of the SOM region (shaded grey) and ECL region (dashed blue) used in this study. Land-based extremes (heat waves and rainfall extremes) were calculated over Australia (colored brown).

the Australian region, *Nicholls et al.* [2010] noted that the SOM used in their study readily produced large-scale features of the circulation but was not able to capture smaller and more transient features of the circulation.

In this paper we extensively test how the end point of the radius training parameter influences the realism of SOM circulation patterns. Focus is also directed toward examining the realism of SOM-derived circulation patterns under different types of meteorological extreme events that impact the Australian region, which appears absent from the literature. The remainder of this paper is structured as follows. Section 2 describes the definitions of extremes, the SOM training procedure, and the methods of SOM analysis. Results are presented in section 3, which are further discussed in section 4, including a case study where we illustrate the utility of SOMs for studying Australian heat waves. Concluding remarks are presented in section 5.

2. Methods

2.1. Data and Definitions of Extreme Events

ERA-Interim [*Dee et al.*, 2011] reanalysis daily MSLP data for years 1979–2015 were primarily used to train SOMs over the Australian region (latitude 10°S to 50°S and longitude 100°E to 170°E; see Figure 1). The original data at 0.75° resolution on a regular grid were interpolated to an Equal-Area Scalable Earth-type grid at a spatial resolution of ~100 km. This interpolation results in SOM input vectors that are weighted by grid cell area and ensures that the correct distance is calculated by the SOM procedure and has been commonly applied in high-latitude regions [*Uotila et al.*, 2007; *Finnis et al.*, 2009; *Lynch et al.*, 2016]. To examine the dependency of results to the reanalysis product chosen, we repeated the analysis by using Modern-Era Retrospective analysis for Research and Applications, Version 2 (MERRA-2) [*Rienecker et al.*, 2011; *Bosilovich et al.*, 2015] MSLP reanalysis data (1980–2015) to train each SOM configuration. The MERRA-2 SOM was trained in an identical manner to the ERA-Interim SOM, which is described in detail below. However, unless otherwise stated, results are presented for the ERA-Interim SOM with comparisons made to MERRA-2 in some sections.

Data from the Australian Water Availability Project (AWAP) data sets [*Jones et al.*, 2009] were used to calculate heat waves and heavy rainfall events on a grid point basis. Among other variables, the AWAP data set provides high-resolution daily gridded temperature and rainfall fields constructed through spatial interpolation of all available stations across Australia managed by the Bureau of Meteorology. For parts of the arid central/western Australia the lack of station-based observations renders the gridded data set less reliable in this region, and it is subsequently not included when defining days on which extreme events occur or is masked out when these data are mapped. The masked region applied to the AWAP data set is the same as that used by *Perkins et al.* [2015].

Heat waves were calculated according to the excess heat factor (EHF) definition [*Nairn and Fawcett*, 2015] which is well suited to the Australian region [*Perkins and Alexander*, 2013], and since the definition is discussed in detail in those references, it is only conceptually introduced here. This definition is based on daily average temperature exceeding the 90th percentile of the base period daily temperature for 3 calendar days. The base period temperature percentiles are computed from a 15 day moving window over the period of 1961–1990 on a grid point basis, as in *Perkins and Alexander* [2013]. The Austral Australian summer heat wave season is often considered to comprise months November through March (NDJFM) [e.g., *Perkins and Alexander*, 2013], so we follow this convention. For completeness, heat waves were also considered over an extended Austral winter heat wave season May through September (MJJAS) (sometimes referred to as "winter warm spells") [e.g., *Cowan et al.*, 2014]. Rainfall extremes (i.e., heavy rainfall) were defined in this

study as exceeding the 95th percentile of the base period rainfall for a single day. As with heat waves, the base period rainfall percentiles were computed over a 15 day moving window for the period of 1961–1990. These choices, while somewhat arbitrary, ensure that both the seasonal cycle is accounted for and a reasonable sample size is retained. Sensitivity testing to other reasonable lengths of the 15 day moving window (e.g., 10 days or 20 days) suggested that our results are robust to this choice.

Heat waves and heavy rainfall event days (HW and R95, respectively) were then defined as a day in which 10% (area-weighted) or more of the Australian continent, in any location, is experiencing these occurrences. This filters out very spatially constrained occurrences while still retaining a reasonably large minimum sample size (the minimum sample size was 873 event days over the period of 1979–2015). For defining R95 events, only grid points south of 20° latitude were included to give focus to the midlatitudinal circulation. This is because MLSP-based classifications for this region [e.g., *Brown et al.*, 2010; *Alexander et al.*, 2010] more readily give rise to patterns that characterize the west-to-east progression of cyclones and frontal systems within the "storm track" region which are strongly linked to rainfall and rainfall extremes for southern Australia [*Catto and Pfahl*, 2013]. In contrast, rainfall in Australia's tropical north is highly seasonal and related to the summer monsoon and other variables such as upper atmosphere wind and vertical thermodynamic profiles are important for characterizing these processes [*Pope et al.*, 2009].

The third type of extreme event considered was east coast lows (ECLs). ECLs are closed low-pressure systems that form off the east coast of Australia and are known to cause heavy rainfall and flooding across coastal southeast Australia [*Pepler et al.*, 2014]. ECLs were identified and tracked with a widely used low tracking scheme applied to the 6-hourly ERA-Interim MSLP data [*Murray and Simmonds*, 1991; *Simmonds et al.*, 1999; *Lim and Simmonds*, 2007]. This automated method was found to have good skill in identifying observed ECLs by *Pepler et al.* [2015] and is described further therein. Briefly, a low is considered to be an ECL if it maintains a closed center with a Laplacian above 1 hPa deg lat^{-2} averaged within 2° of the low center for at least 6 h and crosses through a region bound by the east coast and latitude 24°S to 41°S (Figure 1). A day is considered an "ECL day" if an ECL is present within this region at any point on the day, with ECLs present on an average of 35 days per year.

2.2. SOM Analysis

The SOM training procedure was briefly introduced in section 1 and since a number of existing papers have comprehensively detailed the SOM algorithm, and how it is commonly applied in climatology [e.g., *Hewitson and Crane*, 2002; *Sheridan and Lee*, 2011], we shall instead direct focus to the specifics of the SOM training procedure used in this study for purposes of reproducibility. The sensitivity of the final SOMs to the end point of the radius parameter was tested by training two sets of SOMs. Broadly following *Jiang et al.* [2015] we define SOM-p and SOM-c as SOMs for "projections" and SOMs for "clustering," respectively. This terminology reflects the intention of the user for whether the primary focus is on SOMs for projections or SOMs for clustering, as discussed in section 1. Set SOM-p was trained with a start-point radius of 5 that decreases linearly to end point radius of 1. Set SOM-c was trained with 50% of iterations under a radius that decreases linearly from 5 to 1 with the remaining 50% of iterations at a radius set to 1. We also point out that in the "Kohonen" package for R, used in this study, a radius value of 1 corresponds to the point where only the winning node is updated in training. This may arbitrarily differ in convention from other SOM software where this value is 0 [e.g., *Jiang et al.*, 2015].

For both SOM-p and SOM-c training approaches the other training parameters were held constant to allow comparisons to be made directly in terms of end point of the radius parameter. In particular, the SOM grid topology was hexagonal and a Euclidean distance measure was used. Training was carried out with 5000 iterations and with the start-point of the learning rate at 0.05 (and decreased linearly to 0) and the start-point of the radius at 5. The random initialization scheme was also used. Further sensitivity testing revealed that changes to different combinations of other training parameters had relatively little influence (consistent with results presented elsewhere) in comparison to changes to the radius end point. For completeness, we also train our SOMs with various $x \times y$ configurations (where x and y refer to the number of horizontal and vertical nodes in the 2-D SOM plane, respectively) including 2×3, 4×5, 5×6, and 6×7. For each node configuration, SOMs were separately trained for extended summer (NDJFM) and winter (MJJAS) periods.

To examine the "realism" of the SOMs we compute the Pearson pattern correlation between each winning node pattern and the observed MSLP field at that daily time step. Analysis of the distribution of all daily

pattern correlations is then carried out to quantify the overall accuracy represented by the node patterns; a similar procedure was used by *Feldstein and Lee* [2014] to inform a decision regarding the size of the SOM configuration. We further examine these distributions of pattern correlations under subsets of days for different types of extreme events. Our motivation for doing so is as follows. The patterns obtained in previous studies applying SOMs to the region [e.g., *Brown et al.*, 2010; *Alexander et al.*, 2010] suggest that SOMs tend to produce rather generalized and smoothed features of the circulation. While this may provide a reasonable characterization of the circulation on typical days, the realism of such smoothed patterns would potentially be reduced during extreme events that are related to less typical meteorological conditions (e.g., ECLs).

To evaluate differences in distributions of pattern correlations between particular sets of conditions (i.e., different SOMs training approach or extreme event) we calculate the two-sample Kolmogorov-Smirnov test (KS test) with one-sided bootstrapped (with 5000 simulations) *P* values. A known limitation of the KS test is that potentially relevant differences in the distributions can occur outside of where the KS test statistic is calculated [*Scholz and Stephens*, 1987; *Engmann and Cousineau*, 2011]. Given this, we further calculated the two-sample Anderson Darling test (AD test) which considers differences across the entire sample distributions and can be more sensitive to differences in the distribution tails. To assess the significance of the AD test we perform 5000 permutations based on random splits of the pooled samples to estimate the two-sided *P* values [*Scholz and Stephens*, 1987]. In this study the KS test is used to test the hypothesis that one distribution is stochastically larger than the other, and the nondirectional AD test is used to test the hypothesis that distributions are drawn from a common population. In both approaches, significance is determined at the 5% level.

As in *Horton et al.* [2015], to consider the uniqueness of SOM patterns in a given SOM configuration, we also examine pattern correlations between n pairs of node patterns ($n = N[N-1]/2$, where N is the number of nodes). For example, under the 2×3 configuration (6 nodes), 15 pattern correlations are computed and the distribution of these values is considered as a measure of node pattern uniqueness. To extend this we also apply the false discovery rate (FDR) approach to test for "field significance" [*Wilks*, 2006] in consideration of whether any of the pattern pairs are statistically indistinguishable from each other. The FDR criterion for field significance requires at least one local test (of all the tests calculated per grid point between the pattern pairs) to be significant above a certain threshold by controlling the expected proportion of local null hypothesis that are falsely rejected. This has been suggested as a way to impose an upper limit on SOM size [*Johnson*, 2013], since the SOM should not be too large that some patterns become statistically indistinguishable from each other. Here we also choose the FDR control level as 5%. To summarize, pattern correlations in this study are used in two different ways. First, to measure the realism of node patterns calculated between the winning node and the observed MSLP field at that daily time step, and second, to measure the uniqueness of SOM patterns calculated between all node pairs.

Sammon mapping [*Sammon*, 1969], which is a form of multidimensional scaling, is an effective way to visualize the closeness of nodes in 2-D space. Sammon maps were used in this study to compare the degree of self-organization of nodes between training methods SOM-c and SOM-p. The topological error (TE) defined as the average geometric distance between the winning and second best matching node was also calculated. Therefore, a lower TE indicates a more topologically ordered (i.e., more "self-organized") SOM plane.

Lastly, odds ratios were used to examine the association between circulation represented in the SOM node patterns and heat wave day occurrence. The odds ratio is computed as the odds that an outcome will occur (i.e., heat wave day) given a particular exposure (i.e., particular SOM node pattern) divided by the odds that an outcome will occur in the absence of that exposure. The FDR was also applied on a grid point basis to the *P* value field of the odds ratios.

3. Results

The expectation that SOM-c may produce more distinct circulation patterns is quantitatively examined in Figure 2. In both seasons, the distribution of pattern correlations from all node pairs under various node configurations is found to be typically lower for method SOM-c. Most apparent is the reduction in the minimum pattern correlation indicating that at least one more unique pattern has been introduced in each node configuration tested. This finding is also robust to the reanalysis product chosen, with similar results presented in Figure S1 in the supporting information for MERRA-2.

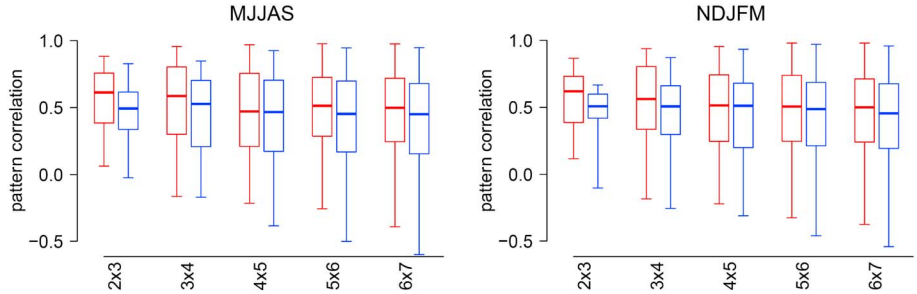

Figure 2. Boxplots of pattern correlations between all node pair patterns. The blue color is method SOM-c, while the red color is SOM-p. In all node configurations for both SOM-c and SOM-p, the number of statistically indistinguishable pairs according to the FDR was zero. Low or negative pattern correlation values suggest the addition of rarer or more unique node patterns.

To illustrate this further, the winter (i.e., Austral winter) node patterns for a 30 node SOM trained under methods SOM-p and SOM-c are shown in Figures S2 and S3, respectively. As an example, node pattern a3 (Figure S3) resembles an isolated ECL in the Tasman Sea which is not evident in any of the SOM-p node patterns. This exemplifies how the SOM-c method is capable of representing synoptic situations that occur less frequently, whereas the SOM-p method, by the nature of the training procedure, may smooth out such features. The implications of this in terms of how realistically each method is capable of representing the circulation during different extremes are examined further in this section. However, another consequence of the SOM-c training is that the close arrangement of similar nodes in the 2-D SOM array has been reduced (Figure 3). This is evident in the higher TE value for SOM-c compared to SOM-p and also in the Sammon mapping of nodes, whereby the corner nodes of the SOM plane (i.e., nodes a0, a4, d0, and d4) do not map to the corners of the Sammon map. Similar results were found for other node configurations and also in MJJAS (not shown).

In terms of the maximum pattern correlations in Figure 2, no node pairs were found to be statistically indistinguishable from each other in either the SOM-c or SOM-p cases. This suggests that even for the largest SOM configuration examined in this study (i.e., 42 nodes in a 6×7 configuration) the addition of new nodes does not necessarily become redundant. Though, at some point, beyond 42 nodes, the addition of new nodes may become redundant, but this was not examined here.

Turning toward node realism, Figure 4 displays CDFs of distributions of pattern correlations for the daily observed MSLP pattern against the node pattern to which that day was assigned. For all node configurations tested, it is found that method SOM-c produces node patterns that more closely resemble (i.e., larger pattern correlation) the observed MSLP for a greater number of days in summer months. The improved pattern

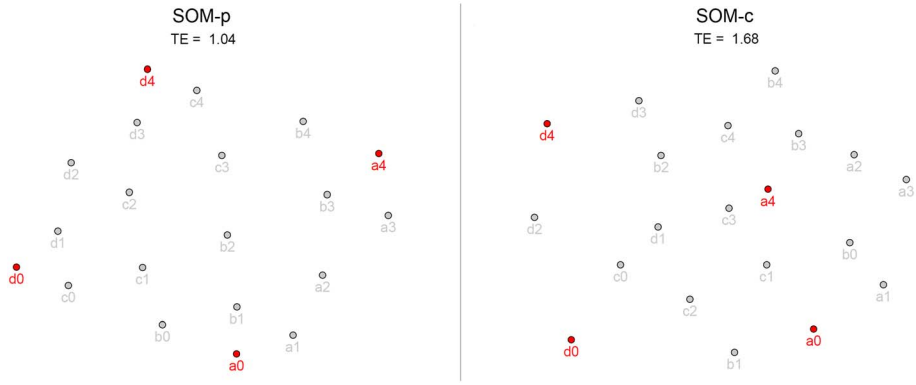

Figure 3. Sammon mapping of training methods SOM-p and SOM-c under a 20-node configuration for NDJFM. The between-node distances in the two-dimensional Sammon map represent the Euclidean distances between nodes in the SOM plane. The nodes colored red represent the four corners of the SOM plane. A lower topological error (TE) represents a higher degree of self-organization of nodes in the SOM plane. For further reference, SOM node labels are shown in Figure 8 for SOM-c.

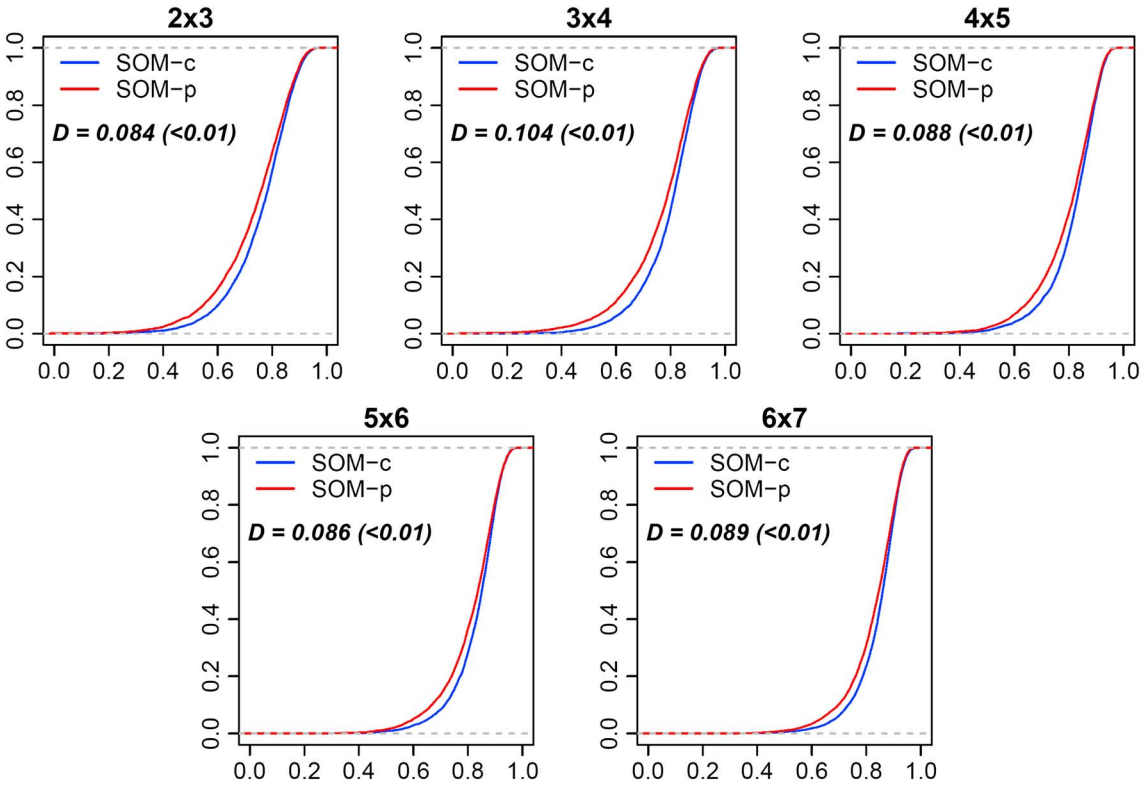

Figure 4. Cumulative distribution functions (CDFs) for NDJFM pattern correlations (see section 2) for the different SOM training methods and for different-sized node configurations. The KS test distance value (*D*) is given, which calculates the maximum absolute difference between each CDF; *P* value is given in brackets. In all cases the KS test suggests that distributions of pattern correlations for method SOM-c are stochastically larger than distributions for method SOM-p. In all cases the AD test also suggests that distributions are drawn from different populations.

realism under method SOM-c is also found when SOM configurations were trained with MERRA-2 reanalysis (Figure S4) and also suggests that this result is not sensitive to the choice of reanalysis.

These results are then extended to examine different types of extreme events in both summer and winter months (Figure 5). For all types of extreme event considered, the SOM-c method is found to produce

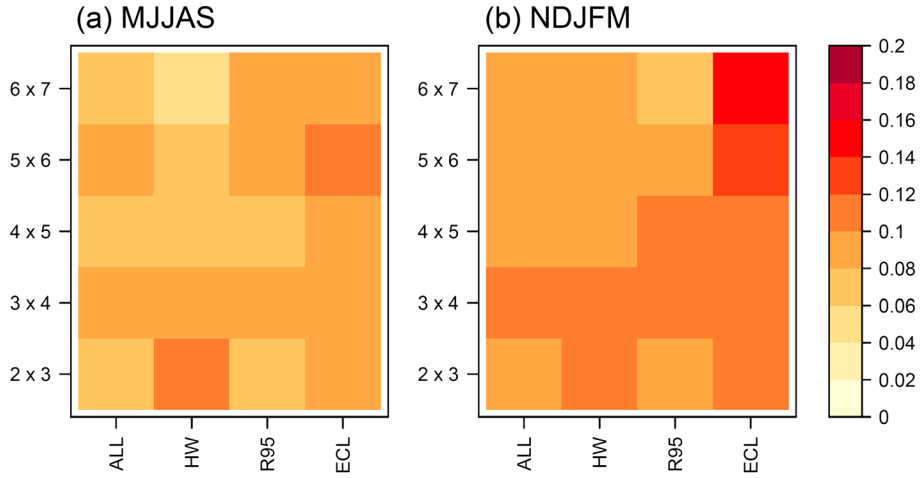

Figure 5. KS test distance value (*D*) comparing SOM-c and SOM-p methods for (a) winter and (b) summer and for different node configurations and subsets by extremes. In all cases the KS test suggests that distributions of pattern correlations for method SOM-c are stochastically larger (i.e., more realistic) than distributions for method SOM-p. Note that the "ALL" case in Figure 5b is the same as the *D* values presented in Figure 4 for NDJFM. In all cases the AD test also suggests that distributions are drawn from different populations.

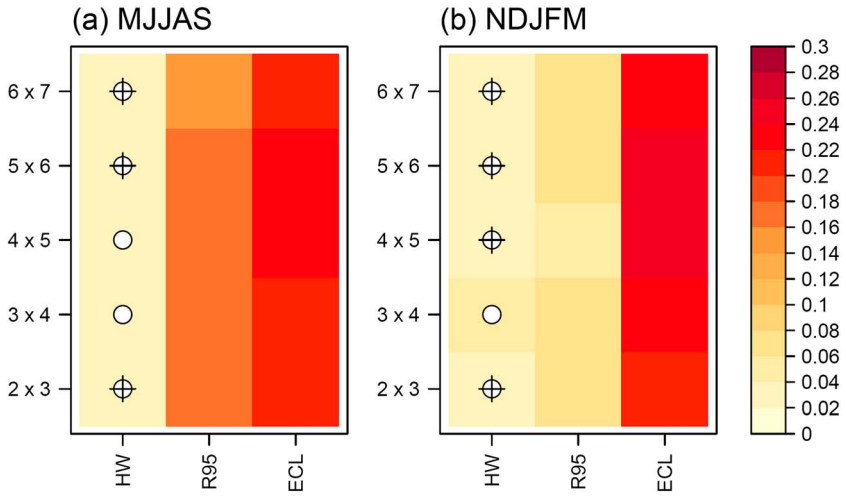

Figure 6. KS test distance value (*D*) comparing distributions of pattern correlations for particular extremes (i.e., HW, R95, and ECL) versus "all days." The white circle indicates no evidence that distributions of pattern correlations for "all days" are stochastically larger (i.e., more realistic) than distributions for the particular extreme considered under the KS test. The white circle with cross indicates evidence that distributions are also drawn from a common population under the AD test. Note that the color bar range is different to that in Figure 5.

more realistic (at 5% significance) node patterns, with this result insensitive to the season or node configuration. Typically, the improvement is more pronounced for summer and for extreme events. In winter, the largest improvements are for heat wave days under a small 2 × 3 SOM configuration and for ECL under a 5 × 6 configuration. The improvement for winter ECL days under this particular configuration is not surprising, given that patterns beginning to resemble ECL first appear under 30 nodes with method SOM-c (as shown earlier in Figures S2 and S3). Similarly, in summer the largest improvements are for ECL days under large SOM configurations (e.g., 30 nodes and 42 nodes), and relatively large improvements for heat waves and R95 are also shown in more moderately sized SOM configurations (e.g., 12 nodes and 20 nodes). To summarize, we have shown that method SOM-c in comparison to SOM-p tends to produce rarer node patterns that are also more realistic, and this appears to translate to a better characterization of the synoptic conditions that occur during extreme events.

Another relevant question to ask is: although training SOMs through method SOM-c allows for a better representation of extreme events (compared to SOM-p), is the realism of the improved circulation sufficiently adequate to characterize extremes? To study this, we examine how the distributions of node pattern correlations under typical days (i.e., days when a particular extreme does not occur) compare to those during extreme events (Figure 6). Given earlier results, focus is directed toward method SOM-c. In both summer and winter months, for a number of node configurations there is no statistically significant reduction in the realism of circulation during heat wave days under the KS test and further evidence that distributions are drawn from a common population under the AD test. In contrast, R95 and especially ECL days are less realistically represented by SOM node patterns, even for large SOM node configurations. It may seem reasonable to assume that a large-sized SOM, which will include a greater diversity of node patterns, will adequately represent the circulation related to extremes, but this appears not necessarily to be the case. Clearly, these results have implications for studies linking extreme events to SOM node patterns and how these node patterns change in time, which are discussed further in section 4.

Lastly, although we have tested the sensitivity of our results to a range of node configurations, in many applications this is too cumbersome and an "optimal" node number is sought. This is often done in consideration of whether additional nodes significantly improve the realism of patterns, and consideration of this is given in Figure 7. As for earlier considerations (e.g., Figures 5 and 6), results are also presented by season and for different subsets of extremes. It is worth pointing out that adding nodes always improves the realism of node patterns to some extent, provided that the newly added patterns are not statistically indistinguishable from each either (which was shown earlier). As evident in Figure 7, each of the larger SOM node pairs consistently and significantly improves the pattern realism. The improvements are largest when increasing the size of

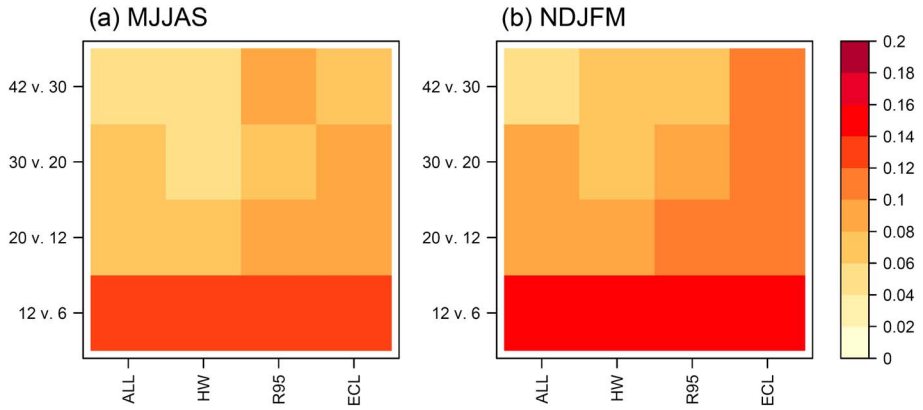

Figure 7. KS test distance value (*D*) comparing distributions of pattern correlations between different SOM configuration pairs (i.e., number of nodes). In all cases the KS test suggests that distributions of pattern correlations for the larger SOM pair are stochastically larger (i.e., more realistic). In all cases the AD test also suggests that distributions are drawn from different populations. Comparisons are for training method SOM-c.

smaller SOMs; for example, increasing the SOM size from 6 nodes to 12 nodes is more beneficial than increasing the SOM size from 30 to 42 nodes. However, the improvements are also dependent on the type of extreme considered, and the benefits for increasing the SOM size are typically greater for ECLs than for heat waves.

4. Discussion

While the advantages of training the SOM with the radius parameter fixed at 1 in the later stages of training (i.e., method SOM-c) have been demonstrated here, a consequence of this is that the array ordering of the SOM nodes is affected. This is not unexpected since the SOM preserves topological features by updating both the winning and surrounding nodes in its neighborhood kernel function throughout training, provided that the radius parameter is greater than 1.

While the "self-organizing" nature of SOMs is often pointed out as a unique and attractive feature of the method [e.g., *Hewitson and Crane*, 2002; *Sheridan and Lee*, 2011], we suggest that for many applications in synoptic climatology this is secondary in importance to producing realistic SOM nodes. This is especially the case when the SOM nodes are subsequently linked to extreme events, where the realism of SOM patterns may be quite limited anyway, and when the SOM size is relatively small. For example, *Horton et al.* [2015] trained SOMs with few enough nodes (i.e., 4 nodes) that similarities between patterns are already readily apparent. When larger sized SOMs are implemented (e.g., 30–40 nodes) it has been suggested that the self-organization of nodes readily allows adjacent nodes to be grouped together to small secondary clusters that span the SOM space [e.g., *Cassano et al.*, 2016]. However, additional clustering methods (e.g., hierarchical clustering, as in *Ohba et al.* [2015]) can also be implemented to group node patterns that represent similar circulation features, so this should not necessarily be viewed as a drawback of the SOM-c method. As an example, Figure S5 shows additional clustering performed on a 30-node SOM trained under method SOM-c, where clusters of nodes that are highly correlated become apparent. It is also worth pointing out that the original motivation for the self-organizing nature of the SOM appeared to stem from training very large SOMs (e.g., several hundred nodes) for exploratory analysis of large data sets [*Kohonen*, 2013] yet, with few exceptions [e.g., *Ohba et al.*, 2015], SOMs are not often used in this fashion in synoptic climatology applications.

As previously noted, at the later stages of training where the radius parameter becomes 1 the SOM algorithm becomes equivalent to the K-means clustering algorithm. Therefore, it may be convenient to view the SOM-c training method as a hybrid approach between SOMs and K-means where the initial features of the nodes are determined by the SOM and the later refinement of more realistic (and more diverse) patterns is achieved through K-means. Some authors have pointed out potential advantages of SOMs over either K-means or empirical orthogonal functions for pattern extraction and cluster analysis of meteorological or oceanographic data [*Huth et al.*, 2008; *Johnson et al.*, 2008; *Johnson*, 2013]. However, comparisons between these methods have not been carried out for the Australian region in the context of weather typing. Although a detailed

comparison between the SOM training approaches and K-means was outside the immediate scope of this study, we briefly examine differences in Figure S6 where additional weather types were obtained by applying K-means clustering through the *Hartigan and Wong* [1979] algorithm with 50 different random initializations per node configuration. As shown in Figure S6, based on the very high degree of similarity of pattern correlation distributions, the K-means algorithm appears to provide no further improvements to pattern realism compared to method SOM-c. However, this also implies that the K-means method is capable of producing more realistic patterns compared to method SOM-p, which has traditionally been applied to the Australian region, and may warrant further consideration.

We have also found that even under method SOM-c the realism of node patterns during heavy rainfall and ECLs is reduced. For ECLs, in both summer and winter, this is most pronounced, and while implementing a larger sized SOM improves the realism, this issue is still present in the largest SOM configuration tested here (42 nodes). For heavy rainfall the reduction in realism, while still found to be statistically significant, is notably smaller, particularly in summer. How important these issues are will of course depend on the specific application of SOMs but appear important enough to warrant careful consideration by relevant users. For example, our results highlight that even for large SOMs, too few patterns are allocated to describing the range of synoptic conditions that occur during ECLs. This does not immediately imply that SOMs cannot be useful for studying ECLs, and some suggestions are briefly discussed which would also be relevant for other types of extreme events and for other regions. First, limiting the spatial domain of the SOM to a more restrained area of interest would limit the variability in the data and could allow the SOM to more readily span rarer synoptic occurrences in that region [e.g., *Cassano et al.*, 2015]. Second, and for a similar reason, the SOM could be trained on the subset of days only when the extreme event occurred. One limitation of this second approach is that the full time series of node patterns is lost which may be important for some applications. Third, the SOM could be trained with variables other than MSLP or with multiple variables (provided that they are normalized before training) that are known to characterize the synoptic situation for the particular extreme event of interest [e.g., *Hope et al.*, 2014; *Swales et al.*, 2016; *Loikith et al.*, 2017].

In contrast to the other extreme events examined here, for heat wave events we find no evidence that the circulation is less well represented compared to days in which heat waves do not occur. This implies that relatively typical features of the day-to-day circulation (in which SOMs appear to more favorably reproduce) are responsible for driving heat waves. This is examined in further detail in Figure 8 which shows the odds ratio of heat wave day occurrence on a grid point basis for each of the SOM nodes.

Collectively, at least in the higher latitudes, the node linkages shown in Figure 8 point toward favorable heat wave conditions at locations positioned to the left and right of high- and low-pressure centers, respectively. This highlights the importance of horizontal temperature advection of relatively warm continental air to coastal regions around Australia produced by the various synoptic situations examined. The primary importance of advection for Australian heat waves appears to differ somewhat compared to many Northern Hemisphere middle-to-high-latitude regions where longer lived [i.e., highly persistent] co-located blocking high-pressure systems are critical to persistent heat wave development [e.g., *Pfahl and Wernli*, 2012].

The linkages reported here for Australia are in broad agreement with other previous studies that have relied on composite analysis to examine the circulation during heat wave days [*Pezza et al.*, 2012; *Purich et al.*, 2014]. With composite analysis, care must be taken to ensure that different synoptic patterns are not being mixed or averaged [*Boschat et al.*, 2016]. While additional steps can be taken to limit this risk, such as a simple "sign" count to assess the directional consistency of patterns used in the construction of the composites [*Grotjahn et al.*, 2016, and references therein], we suggest that the main advantage of weather types lies in the ability to collectively analyze and compare the circulation that co-occurs during extremes at multiple different locations. As pointed out in *Loikith et al.* [2017] this is also valuable for model evaluation, making the evaluation of extremes in multiple models and at multiple locations more manageable through SOMs.

Given the results of the present study, in future work we intend to further examine Australian heat waves within the SOM framework. One caveat to any weather typing procedure is the inherent presence of within-type (i.e., within-node) variability. For example, on a given day, the circulation may be more persistent or more intense than is typical for other days which are classified into the same node. However, we suggest that the use of odds ratios may also be useful for further separating out the relative importance of these contributions. For example, the heat wave odds could be computed by comparing node occurrences that have

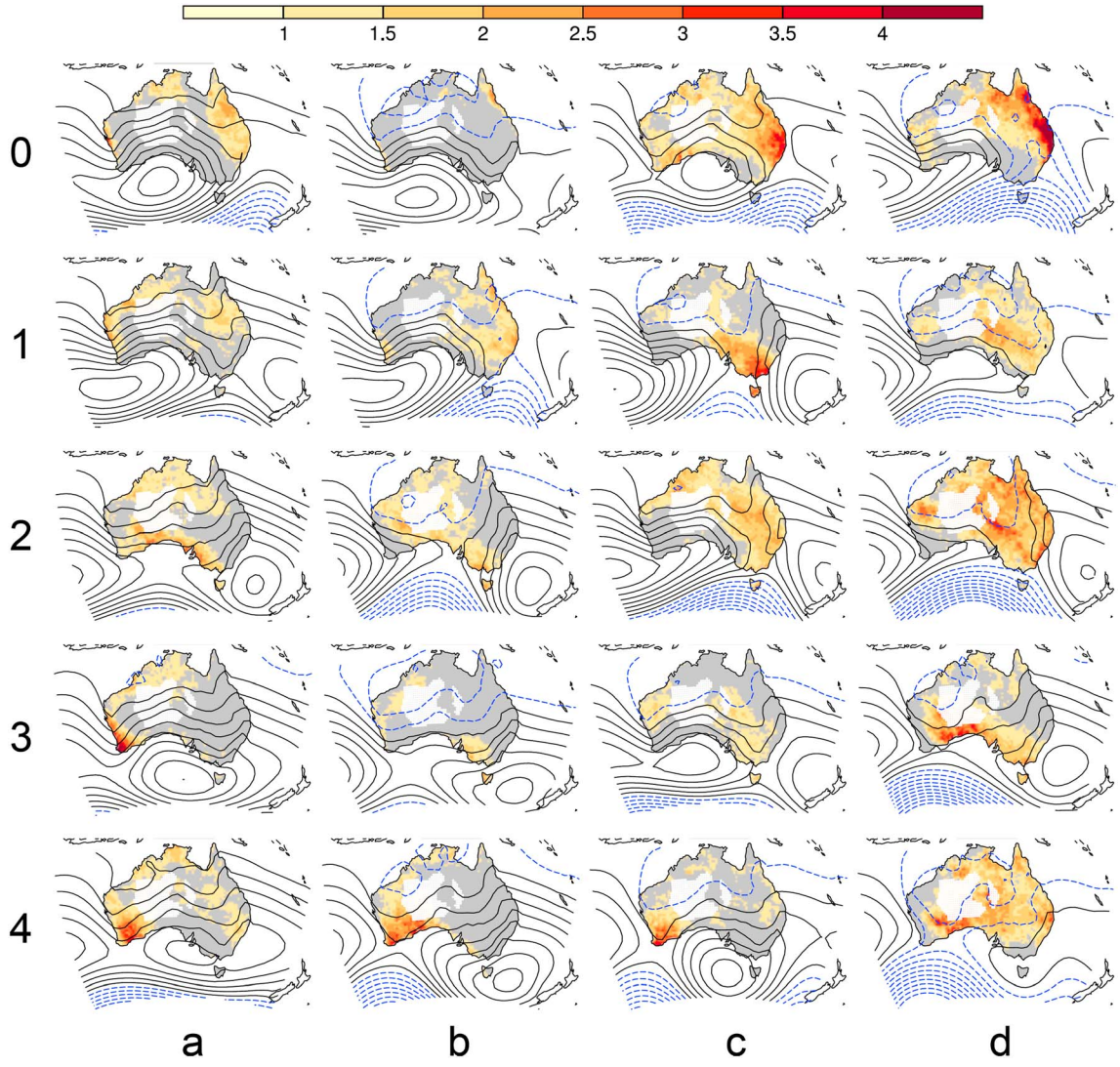

Figure 8. Heat wave odds ratio for method SOM-c (4 × 5) NDJFM nodes. The grid values are shaded according to the odds ratio for each node, where a larger value indicates a larger relative likelihood of heat wave day occurrence. The grid values are masked grey if not greater than 1 and not significant under the FDR criterion. The low station density region in AWAP is masked white. The contours indicate MSLP with contour interval of 2 hPa, the contours greater than or equal to 1010 hPa are black, and the contours less than 1010 hPa are dashed blue. In terms of node referencing, node "a4" refers to the node in the lower left corner of the SOM plane.

persisted for two or more days compared to node occurrences that are more transitional. Another application is land-atmosphere coupling during heat waves. For the Australian region, land surface processes have recently been shown to be important to heat wave conditions in certain parts of Australia [*Hirsch et al.*, 2015; *Perkins et al.*, 2015; *Herold et al.*, 2016] but have not widely been considered in conjunction with atmospheric processes. We suggest that SOMs could be a useful approach for bringing together these somewhat disjointed and important research themes.

5. Conclusions

In this study we have shown how the SOM training procedure can be modified to produce a more diverse range of patterns that are also more realistic and better represent the synoptic conditions during extreme events. However, the approach also reduces the topological SOM ordering. The relative importance of these two factors will depend on the particular user application, but in certain instances, and particularly when the SOM size is relatively small (e.g., 6 nodes or less), it is suggested that the SOM ordering may be of secondary importance.

Even with this improved training procedure, and with a reasonably large sized SOM, the realism of SOM patterns during some types of extreme events is shown to be reduced (compared to the realism on typical days), including heavy rainfall and ECLs. However, this reduction of realism, and how important it is, will depend on the application. This does not immediately imply that SOMs cannot be useful for studying extremes but, at least, the user of SOMs should be aware of these issues when applying SOMs to characterize the circulation that co-occurs during extreme events. Various alternative approaches have also been discussed to circumvent these issues and warrant further research.

For heat waves, the SOM appears to represent the background synoptic conditions well. Analyzing the relative occurrences of heat waves under different SOM nodes has both confirmed past results and added new understanding. Compared to simply analyzing composites of the circulation on days when heat waves occur, SOMs allow multiple locations to be examined comparatively and may reduce the risk of different synoptic patterns being mixed and averaged out. Novel approaches for using SOMs to study heat wave processes have been suggested, including examining land-surface processes in conjunction with atmospheric processes.

Acknowledgments

We thank the NCI National Facility at the Australian National University for providing data storage and computational facilities. We also thank the Australian Bureau of Meteorology (BoM), ECMWF, and NASA GMAO for the provision of data used in this study. The AWAP data used in this study are available upon request from BoM (e.g., see http://www.bom.gov.au/climate/maps). The ERA-Interim and MERRA-2 reanalysis data are freely available and were downloaded from http://apps.ecmwf.int/datasets and http://disc.sci.gsfc.nasa.gov/uui/datasets, respectively. The derived LAPv2 ECL data set can be obtained upon request through author Acacia Pepler (a.pepler@student.unsw.edu.au). The Python code used to calculate EHF heat waves was kindly provided by Tammas Loughran and is available at https://github.com/tammasloughran/ehfheatwaves. The SOM analysis was performed in R by using the "Kohonen" package and is available through https://cran.r-project.org/web/packages/kohonen/index.html. The cluster analysis used in Figure S5 was performed in R by using the "corrplot" package and is available through https://cran.r-project.org/web/packages/corrplot/index.html. All plots were produced by using NCL and R, which are freely available software. This work was supported by the Australian Research Council (ARC) Centre of Excellence for Climate System Science grant CE110001028. Author P.G. was supported by an Australian Postgraduate Award and author S.P.-K. supported by an ARC Discovery Early Career Researcher Award (DE140100952). Author P.U. was supported by a NordForsk project (74456) and by an H2020-MSCA-IF-2015 award (707262).

References

Alexander, L. V., P. Uotila, N. Nicholls, and A. Lynch (2010), A new daily pressure dataset for Australia and its application to the assessment of changes in synoptic patterns during the last century, *J. Clim.*, *23*(5), 1111–1126, doi:10.1175/2009JCLI2972.1.

Bação, F., V. Lobo, and M. Painho (2005), Self-organizing maps as substitutes for K-means clustering, in *Computational Science—ICCS 2005, Lect. Notes Comput. Sci.*, vol. 3516, edited by V. S. Sunderam et al., pp. 476–483, Springer, Berlin.

Boschat, G., I. Simmonds, A. Purich, T. Cowan, and A. B. Pezza (2016), On the use of composite analyses to form physical hypotheses: An example from heat wave-SST associations, *Sci. Rep.*, *6*, 29599, doi:10.1038/srep29599.

Bosilovich, M., et al. (2015), MERRA-2: Initial evaluation of the climate, *NASA Technical Report Series on Global Modeling and Data Assimilation, NASA/TM-2015-104606*, vol. 43, 139 pp., Natl. Aeronaut. and Space Admin., Goddard Space Flight Cent., Greenbelt, Md.

Brown, J. R., C. Jakob, and J. M. Haynes (2010), An evaluation of rainfall frequency and intensity over the Australian region in a global climate model, *J. Clim.*, *23*(24), 6504–6525, doi:10.1175/2010JCLI3571.1.

Cassano, E. N., J. M. Glisan, J. J. Cassano, W. J. Gutowski Jr., and M. W. Seefeldt (2015), Self-organizing map analysis of widespread temperature extremes in Alaska and Canada, *Clim. Res.*, *62*(3), 199–218.

Cassano, J. J., P. Uotila, and A. Lynch (2006), Changes in synoptic weather patterns in the polar regions in the twentieth and twenty-first centuries. Part 1: Arctic, *Int. J. Climatol.*, *26*(8), 1027–1049, doi:10.1002/joc.1306.

Cassano, J. J., E. N. Cassano, M. W. Seefeldt, W. J. Gutowski, and J. M. Glisan (2016), Synoptic conditions during wintertime temperature extremes in Alaska, *J. Geophys. Res. Atmos.*, *121*, 3241–3262, doi:10.1002/2015JD024404.

Catto, J. L., and S. Pfahl (2013), The importance of fronts for extreme precipitation, *J. Geophys. Res. Atmos.*, *118*, 10,791–710,801, doi:10.1002/jgrd.50852.

Cowan, T., A. Purich, S. Perkins, A. Pezza, G. Boschat, and K. Sadler (2014), More frequent, longer, and hotter heat waves for Australia in the twenty-first century, *J. Clim.*, *27*(15), 5851–5871, doi:10.1175/JCLI-D-14-00092.1.

Dee, D. P., et al. (2011), The ERA-Interim reanalysis: Configuration and performance of the data assimilation system, *Q. J. R. Meteorol. Soc.*, *137*(656), 553–597, doi:10.1002/qj.828.

Engmann, S., and D. Cousineau (2011), Comparing distributions: The two-sample Anderson-Darling test as an alternative to the Kolmogorov-Smirnoff test, *J. Appl. Quant. Methods*, *6*(3), 1–17.

Feldstein, S. B., and S. Lee (2014), Intraseasonal and interdecadal jet shifts in the Northern Hemisphere: The role of warm pool tropical convection and sea ice, *J. Clim.*, *27*(17), 6497–6518, doi:10.1175/JCLI-D-14-00057.1.

Finnis, J., J. Cassano, M. Holland, M. Serreze, and P. Uotila (2009), Synoptically forced hydroclimatology of major Arctic watersheds in general circulation models. Part 1: The Mackenzie River basin, *Int. J. Climatol.*, *29*(9), 1226–1243, doi:10.1002/joc.1753.

Gibson, P. B., S. E. Perkins-Kirkpatrick, and J. A. Renwick (2016a), Projected changes in synoptic weather patterns over New Zealand examined through self-organizing maps, *Int. J. Climatol.*, *36*, 3934–3948, doi:10.1002/joc.4604.

Gibson, P. B., P. Uotila, S. E. Perkins-Kirkpatrick, L. V. Alexander, and A. J. Pitman (2016b), Evaluating synoptic systems in the CMIP5 climate models over the Australian region, *Clim. Dyn.*, *47*, 2235–2251, doi:10.1007/s00382-015-2961-y.

Grotjahn, R., et al. (2016), North American extreme temperature events and related large scale meteorological patterns: A review of statistical methods, dynamics, modeling, and trends, *Clim. Dyn.*, *46*(3), 1151–1184, doi:10.1007/s00382-015-2638-6.

Hartigan, J. A., and M. A. Wong (1979), Algorithm AS 136: A k-means clustering algorithm, *J. R. Stat. Soc. Ser. C. Appl. Stat.*, *28*(1), 100–108.

Herold, N., J. Kala, and L. V. Alexander (2016), The influence of soil moisture deficits on Australian heatwaves, *Environ. Res. Lett.*, *11*(6), 064,003.

Hewitson, B., and R. Crane (2002), Self-organizing maps: Applications to synoptic climatology, *Clim. Res.*, *22*(1), 13–26.

Hirsch, A. L., A. J. Pitman, J. Kala, R. Lorenz, and M. G. Donat (2015), Modulation of land-use change impacts on temperature extremes via land-atmosphere coupling over Australia, *Earth Interact.*, *19*(12), 1–24, doi:10.1175/EI-D-15-0011.1.

Hope, P., K. Keay, M. Pook, J. Catto, I. Simmonds, G. Mills, P. McIntosh, J. Risbey, and G. Berry (2014), A comparison of automated methods of front recognition for climate studies: A case study in Southwest Western Australia, *Mon. Weather Rev.*, *142*(1), 343–363, doi:10.1175/MWR-D-12-00252.1.

Horton, D. E., N. C. Johnson, D. Singh, D. L. Swain, B. Rajaratnam, and N. S. Diffenbaugh (2015), Contribution of changes in atmospheric circulation patterns to extreme temperature trends, *Nature*, *522*(7557), 465–469, doi:10.1038/nature14550.

Huth, R., C. Beck, A. Philipp, M. Demuzere, Z. Ustrnul, M. Cahynová, J. Kyselý, and O. E. Tveito (2008), Classifications of atmospheric circulation patterns, *Ann. N. Y. Acad. Sci.*, *1146*(1), 105–152, doi:10.1196/annals.1446.019.

Huva, R., R. Dargaville, and P. Rayner (2015), The impact of filtering self-organizing maps: A case study with Australian pressure and rainfall, *Int. J. Climatol.*, *35*(4), 624–633, doi:10.1002/joc.4008.

Jiang, N., K. Luo, P. J. Beggs, K. Cheung, and Y. Scorgie (2015), Insights into the implementation of synoptic weather-type classification using self-organizing maps: An Australian case study, *Int. J. Climatol.*, *35*(12), 3471–3485, doi:10.1002/joc.4221.
Johnson, N. C. (2013), How many ENSO flavors can we distinguish?, *J. Clim.*, *26*(13), 4816–4827, doi:10.1175/JCLI-D-12-00649.1.
Johnson, N. C., S. B. Feldstein, and B. Tremblay (2008), The continuum of Northern Hemisphere teleconnection patterns and a description of the NAO shift with the use of self-organizing maps, *J. Clim.*, *21*(23), 6354–6371, doi:10.1175/2008JCLI2380.1.
Jones, D. A., W. Wang, and R. Fawcett (2009), High-quality spatial climate data-sets for Australia, *Aust. Meteorol. Oceanogr. J.*, *58*(4), 233.
Kohonen, T. (2013), Essentials of the self-organizing map, *Neural Netw.*, *37*, 52–65, doi:10.1016/j.neunet.2012.09.018.
Lennard, C., and G. Hegerl (2015), Relating changes in synoptic circulation to the surface rainfall response using self-organising maps, *Clim. Dyn.*, *44*(3), 861–879, doi:10.1007/s00382-014-2169-6.
Lim, E.-P., and I. Simmonds (2007), Southern Hemisphere winter extratropical cyclone characteristics and vertical organization observed with the ERA-40 data in 1979–2001, *J. Clim.*, *20*(11), 2675–2690, doi:10.1175/JCLI4135.1.
Liu, Y., R. H. Weisberg, and C. N. K. Mooers (2006), Performance evaluation of the self-organizing map for feature extraction, *J. Geophys. Res.*, *111*, C05018, doi:10.1029/2005JC003117.
Loikith, P. C., and A. J. Broccoli (2015), Comparison between observed and model-simulated atmospheric circulation patterns associated with extreme temperature days over North America using CMIP5 historical simulations, *J. Clim.*, *28*(5), 2063–2079, doi:10.1175/JCLI-D-13-00544.1.
Loikith, P. C., B. R. Lintner, and A. Sweeney (2017), Characterizing large-scale meteorological patterns and associated temperature and precipitation extremes over the northwestern United States using self organizing maps. *J. Clim.*, doi:10.1175/jcli-d-16-0670.1, in press.
Lynch, A. H., M. C. Serreze, E. N. Cassano, A. D. Crawford, and J. Stroeve (2016), Linkages between Arctic summer circulation regimes and regional sea ice anomalies, *J. Geophys. Res. Atmos.*, *121*, 7868–7880, doi:10.1002/2016JD025164.
Murray, R. J., and I. Simmonds (1991), A numerical scheme for tracking cyclone centres from digital data. Part I: Development and operation of the scheme, *Aust. Meteorol. Mag.*, *39*, 155–166.
Nairn, J. R., and R. J. Fawcett (2015), The excess heat factor: A metric for heatwave intensity and its use in classifying heatwave severity, *Int. J. Environ. Res. Public Health*, *12*(1), 227–253, doi:10.3390/ijerph120100227.
Nicholls, N., P. Uotila, and L. Alexander (2010), Synoptic influences on seasonal, interannual and decadal temperature variations in Melbourne, Australia, *Int. J. Climatol.*, *30*(9), 1372–1381, doi:10.1002/joc.1965.
Ohba, M., S. Kadokura, Y. Yoshida, D. Nohara, and Y. Toyoda (2015), Anomalous weather patterns in relation to heavy precipitation events in Japan during the Baiu season, *J. Hydrometeorol.*, *16*(2), 688–701, doi:10.1175/jhm-d-14-0124.1.
Pepler, A., A. Coutts-Smith, and B. Timbal (2014), The role of east coast lows on rainfall patterns and inter-annual variability across the East Coast of Australia, *Int. J. Climatol.*, *34*(4), 1011–1021, doi:10.1002/joc.3741.
Pepler, A. S., A. D. Luca, F. Ji, L. V. Alexander, J. P. Evans, and S. C. Sherwood (2015), Impact of identification method on the inferred characteristics and variability of Australian east coast lows, *Mon. Weather Rev.*, *143*(3), 864–877, doi:10.1175/MWR-D-14-00188.1.
Perkins, S. E., and L. V. Alexander (2013), On the measurement of heat waves, *J. Clim.*, *26*(13), 4500–4517, doi:10.1175/JCLI-D-12-00383.1.
Perkins, S. E., D. Argüeso, and C. J. White (2015), Relationships between climate variability, soil moisture, and Australian heatwaves, *J. Geophys. Res. Atmos.*, *120*, 8144–8164, doi:10.1002/2015JD023592.
Pezza, A. B., P. van Rensch, and W. Cai (2012), Severe heat waves in Southern Australia: Synoptic climatology and large scale connections, *Clim. Dyn.*, *38*(1), 209–224, doi:10.1007/s00382-011-1016-2.
Pfahl, S., and H. Wernli (2012), Quantifying the relevance of atmospheric blocking for co-located temperature extremes in the Northern Hemisphere on (sub-)daily time scales, *Geophys. Res. Lett.*, *39*, L12807, doi:10.1029/2012GL052261.
Pope, M., C. Jakob, and M. J. Reeder (2009), Regimes of the North Australian wet season, *J. Clim.*, *22*(24), 6699–6715, doi:10.1175/2009JCLI3057.1.
Purich, A., T. Cowan, W. Cai, P. van Rensch, P. Uotila, A. Pezza, G. Boschat, and S. Perkins (2014), Atmospheric and oceanic conditions associated with southern Australian heat waves: A CMIP5 analysis, *J. Clim.*, *27*(20), 7807–7829, doi:10.1175/JCLI-D-14-00098.1.
Rienecker, M. M., et al. (2011), MERRA: NASA's modern-era retrospective analysis for research and applications, *J. Clim.*, *24*(14), 3624–3648, doi:10.1175/JCLI-D-11-00015.1.
Sammon, J. W. (1969), A nonlinear mapping for data structure analysis, *IEEE Trans. Comput.*, *100*(5), 401–409.
Scholz, F. W., and M. A. Stephens (1987), K-sample Anderson-Darling tests, *J. Am. Stat. Assoc.*, *82*(399), 918–924, doi:10.1080/01621459.1987.10478517.
Sheridan, S. C., and C. C. Lee (2011), The self-organizing map in synoptic climatological research, *Prog. Phys. Geogr.*, *35*(1), 109–119, doi:10.1177/0309133310397582.
Simmonds, I., R. J. Murray, and R. Leighton (1999), A refinement of cyclone tracking methods with data from FROST, *Aust. Meteorol. Mag.*, 35–49.
Swales, D., M. Alexander, and M. Hughes (2016), Examining moisture pathways and extreme precipitation in the U.S. intermountain west using self-organizing maps, *Geophys. Res. Lett.*, *43*, 1727–1735, doi:10.1002/2015GL067478.
Uotila, P., A. H. Lynch, J. J. Cassano, and R. I. Cullather (2007), Changes in Antarctic net precipitation in the 21st century based on Intergovernmental Panel on Climate Change (IPCC) model scenarios, *J. Geophys. Res.*, *112*, D10107, doi:10.1029/2006JD007482.
Wilks, D. S. (2006), On "field significance" and the false discovery rate, *J. Appl. Meteorol. Climatol.*, *45*(9), 1181–1189, doi:10.1175/JAM2404.1.